Published OnlineFirst October 29, 2020; DOI: 10.1158/0008-5472.CAN-20-1994

Lipopolysaccharide-Mediated Chronic Inflammation Promotes Tobacco Carcinogen–Induced Lung Cancer and Determines the Efficacy of Immunotherapy

Chia-Hsin Liu[1,2], Zhong Chen[3], Kong Chen[4], Fu-Tien Liao[1], Chia-En Chung[1], Xiaoping Liu[1,5], Yu-Chun Lin[6], Phouthone Keohavong[1], George D. Leikauf[1], and Yuanpu Peter Di[1]

ABSTRACT

Chronic obstructive pulmonary disease (COPD) is an inflammatory disease that is associated with increased risk of lung cancer. *Pseudomonas aeruginosa* (PA) infections are frequent in patients with COPD, which increase lung inflammation and acute exacerbations. However, the influences of PA-induced inflammation on lung tumorigenesis and the efficacy of immune checkpoint blockade remain unknown. In this study, we initiated a murine model of lung cancer by treating FVB/NJ female mice with tobacco carcinogen nitrosamine 4-(methylnitrosamino)-1-(3-pyridyl)-1-butanone (NNK) alone or in combination with PA-lipopolysaccharide (LPS). LPS-mediated chronic inflammation induced T-cell exhaustion, increased the programmed cell death-1 (PD-1)/programmed cell death ligand-1 (PD-L1) axis, and enhanced NNK-induced lung tumorigenesis through an immunosuppressive microenvironment characterized by accumulation of myeloid-derived suppressive cells (MDSC) and regulatory T cells. Anti–PD-1 antibody treatment reduced tumors in NNK/LPS-treated mice with a 10-week LPS treatment but failed to inhibit tumor growth when LPS exposure was prolonged to 16 weeks. Anti-Ly6G antibody treatment coupled with depletion of MDSC alone reduced tumor growth; when combined with anti–PD-1 antibody, this treatment further enhanced antitumor activity in 16-week NNK/LPS-treated mice. Immune gene signatures from a human lung cancer dataset of PD-1 blockade were identified, which predicted treatment responses and survival outcome and overlapped with those from the mouse model. This study demonstrated that LPS-mediated chronic inflammation creates a favorable immunosuppressive microenvironment for tumor progression and correlates with the efficacy of anti–PD-1 treatment in mice. Immune gene signatures overlap with human and mouse lung tumors, providing potentially predictive markers for patients undergoing immunotherapy.

Significance: This study identifies an immune gene signature that predicts treatment responses and survival in patients with tobacco carcinogen–induced lung cancer receiving immune checkpoint blockade therapy.

Introduction

Lung cancer is the leading cause of cancer-related deaths worldwide with a 5-year survival rate of 19% (1). Non–small cell lung cancer (NSCLC) accounts for approximately 85% of lung cancer, with adenocarcinoma and squamous cell carcinoma being the most common subtypes (2). Tobacco smoking is a well-established risk factor for lung cancer and the main cause of chronic obstructive pulmonary disease (COPD; ref. 3). COPD is characterized by chronic airway inflammation, and patients with COPD have an increased risk for lung cancer even after controlling for smoking (3). This suggests that COPD is an independent risk factor of lung cancer, which provides a plausible link between inflammation and lung cancer.

Pseudomonas aeruginosa (PA), a gram-negative bacterium, colonized in the airway of patients with COPD. A constituent of the PA cell membrane, lipopolysaccharide (LPS) triggers an innate immune response, which correlates with increased inflammation and acute exacerbations in patients with COPD (4). "Smoldering" inflammation in the tumor microenvironment produces tumor-promoting effects by enhancing tumor-cell migration, invasion, metastasis, epithelial–mesenchymal transition, and angiogenesis (5). In addition, chronic inflammation also induces immunosuppression associated with accumulated myeloid-derived suppressor cells (MDSC) and regulatory T cells (Treg), and increased production of related cytokine mediators (e.g., IL10 and TGFβ; ref. 6). However, the mechanisms of bacteria-related chronic inflammation on lung tumorigenesis remain unclear.

Local immune responses and systematic inflammation may not only influence tumor progression but also alter treatment effectiveness (7). Immunotherapy, such as checkpoint inhibitors, has emerged as a valued modality in lung cancer treatment and yielded sustained clinical responses (8, 9). However, the overall treatment response rate in NSCLC is around 15% to 20%, and a deficiency exists for biomarkers that are able to distinguish the responders from nonresponders (10). Survival is increased in programmed cell death-1 (PD-1) blockade recipients among patients with NSCLC with COPD, suggesting that COPD-related inflammation affects treatment efficacy (11, 12). However, the mechanism of effective

[1]Department of Environmental and Occupational Health, Graduate School of Public Health, University of Pittsburgh, Pittsburgh, Pennsylvania. [2]Division of Pulmonary and Critical Care Medicine, Department of Internal Medicine, Tri-Service General Hospital, National Defense Medical Center, Taipei, Taiwan. [3]Tumor Biology Section and Clinical Genomics Unit, Head and Neck Surgery Branch, National Institute on Deafness and Other Communication Disorders, National Institutes of Health, Bethesda, Maryland. [4]Division of Pulmonary, Allergy, and Critical Care Medicine, Department of Medicine, University of Pittsburgh, Pittsburgh, Pennsylvania. [5]Medical College of Qingdao University, Shandong Province, China. [6]Department of Pathology, Tri-Service General Hospital, National Defense Medical Center, Taipei, Taiwan.

Note: Supplementary data for this article are available at Cancer Research Online (http://cancerres.aacrjournals.org/).

Corresponding Author: Yuanpu Peter Di, University of Pittsburgh, 130 Desoto Street, GSPH 4139, Pittsburgh, PA 15261. Phone: 412-624-8718; Fax: 412-624-9361; E-mail: peterdi@pitt.edu

Cancer Res 2021;81:144–57

doi: 10.1158/0008-5472.CAN-20-1994

Published OnlineFirst October 29, 2020; DOI: 10.1158/0008-5472.CAN-20-1994

immunotherapy remains unknown, and current biomarkers only partially predicted response rates. This leaves a significant gap between the current diagnosis and the prognoses for patients with lung cancer under immunotherapy.

Recently, immune gene signatures of transcripts encoding cell surface markers, cytokines, cell signaling molecules, and transcription factors have been discovered that identify specific immune-related responses (13). These immune gene signatures include those that have been associated with clinical responses in a subset of patients with solid tumors after treated with checkpoint inhibitors (14–16). However, the value of these immune gene signatures has been hampered by the complex nature of the tumor and immune cell interactions that are dynamically altered during the different phases of tumor growth. This creates a challenge to identify accurate immune gene signatures for predicting responses to immunotherapy and patient survival. This challenge could be partially addressed by identifying temporal immune gene signatures in the animal models that can be compared with those of patients with lung cancer.

To investigate the impact of chronic inflammation on lung tumorigenesis, we developed a two-staged murine model of lung cancer. This model mimics smoking carcinogen–induced and COPD-related, inflammation-promoted human lung cancers. The model was established using 4-(methylnitrosamino)-1-(3-pyridyl)-1-butanone (aka Nicotine-derived Nitrosamine Ketone: NNK) to generate genetic instability, and repeated LPS treatment to induce chronic inflammation. This exposure paradigm creates an immunosuppressive microenvironment favorable of tumor progression similar to that of inflammation-associated lung tumorigenesis in patients with COPD. Using this model, we examined the immune gene signature, cellular components, and cytokines produced in the tumor microenvironment. In addition, we investigated the efficacy of anti–PD-1 immunotherapy alone and in combination with MDSC depletion to eliminate the immunosuppressive cellular components. We demonstrated that the selected immune gene signatures provide potential markers for predicting responses of patients with NSCLC under immunotherapy.

Materials and Methods

Murine model and reagents

FVB/NJ (7 weeks, female) mice (RRID:IMSR_JAX:001800) were purchased from The Jackson Laboratory. Procedures were approved by the Institutional Animal Use and Care Committee of the University of Pittsburgh (#17081148). LPS from PA (L9143, Sigma) was resuspended and diluted in PBS. NNK (M325750, Toronto Research Chemicals) was dissolved in methanol and diluted in PBS. Mice were treated with PBS, 3 mg NNK (i.p., biweekly for 4 weeks), 5 μg LPS [intranasal instillation (i.n.), weekly for 16 weeks], or combined NNK and LPS (**Fig. 1A**; ref. 17). In addition, mice exposed to NNK with/without 10-week LPS instillation were treated with 200μg i.p. IgG2a (2A3, BioXCell, RRID:AB_1107769), 200 μg i.p., anti–PD-1 (RMP1–14, BioXCell, RRID:AB_10949053), and 200 μg i.p. once weekly for 6 weeks (**Fig. 5A**). Combined NNK and 16-week LPS exposed mice were treated with 200 μg i.p. IgG2a, 200 μg i.p. anti–PD-1, 200 μg i.p. anti-Ly6G (1A8, BioXCell, RRID:AB_1107721) or in combination (**Fig. 5C**). Mice were euthanized 1 week after the last treatment, and samples were obtained for transcript, protein, histopathologic, and IHC analyses. Additional details on methods are presented in the online supplement, and the study flowchart is in Supplementary Fig. S1A to S1C.

Human immune gene signature analysis

The normalized mRNA of 730 immune-related genes and patient profiles were previously obtained under an Institutional Review Board–approved protocol, with informed consents downloaded from the publicly available GSE93157 cohort (15). Tumor samples from 22 nonsquamous (non-SqNSCLC) and 13 squamous NSCLC (SqNSCLC) before anti–PD-1 treatment were analyzed (Supplementary Table S1). The tumor responsiveness to anti–PD-1 treatment was classified as nonprogressive disease (NPD), which included stable disease (SD), partial response (PR), complete response (CR), or progressive disease (PD) based on modified RECIST 1.1 criteria (18). Differentially expressed transcripts ($n = 130$, absolute fold change > 1.5 and unadjusted $P < 0.05$) between NPD and PD were determined using Partek Genomics Suite (RRID:SCR_011860) and assigned as immune gene panel (Supplementary Table S2). Immune gene signatures for T-cell, B-cell, and natural killer (NK) cell were defined by the transcripts, which were present in two or more studies of eight published signatures (Supplementary Table S2; refs. 13, 19–25). IL17 and IL22 were selected as the Th17 cell signature (25). In GSE93157, the median gene level from the immune signature was used for the expressional level quantification. The expression value of each patient was sorted from low to high, and patients were classified into two groups (high vs. low) based on the cutoff value of the signature. The best expression cutoff referred to the signature value that yielded maximal survival differences between the two groups at the lowest log-rank *P* value.

Mouse microarray and immune gene signature analysis

RNA extraction was performed using Trizol (Sigma Chemical). RNA purity and integrity of samples were assessed by Bioanalyzer (Agilent). The cDNA was synthesized and hybridized onto HD Whole Mouse Genome Microarray (Agilent, G2519F-014868). Partek Genomics Suite (Partek) was used to process the raw microarray data, and Robust Multi-array Average method was used for background correction. Differential expression analysis between NNK/LPS and NNK was performed using Partek Genomics Suite, and the Benjamini–Hochberg method was used to adjust the raw *P* values for multiple testing. The transcript threshold was set at ≥ 2 or ≤ -2-fold and FDR < 0.05 for differentially expressed genes (DEG). The hierarchical clustering heatmap was conducted using Partek Genomics Suite. Data are deposited in the Gene Expression Omnibus database (GSE132661, RRID:SCR_005012). Mouse ortholog genes to human immune signature transcripts for immune gene panel, T cell, B cell, NK cell, and Th17 cell identified from published signatures (13, 19–25) were selected with the species conversion tools from Ensembl (www.ensembl.org; RRID:SCR_002344; Supplementary Table S2; ref. 26). We used the mouse granulocytic MDSC gene signature (Supplementary Table S2) as identified by Fridlender and colleagues (27). The median gene level from the immune signature was used for the expressional level quantification.

Statistical analyses

According to data distribution, a parametric test (ANOVA, Student *t* test) or a nonparametric test (Kruskal–Wallis, Mann–Whitney), with appropriate *post-hoc* comparisons, was used to compare quantitative variables across the different groups. Survival was compared using the Kaplan–Meier analysis. The log-rank test was used to compare survival or event-free survival between groups. Calculation of the area under the ROC curve was used as a measure of discriminatory ability for the immune gene signatures. The χ^2 test was used to compare frequencies in one or more categories. $P < 0.05$ was considered significant.

Published OnlineFirst October 29, 2020; DOI: 10.1158/0008-5472.CAN-20-1994

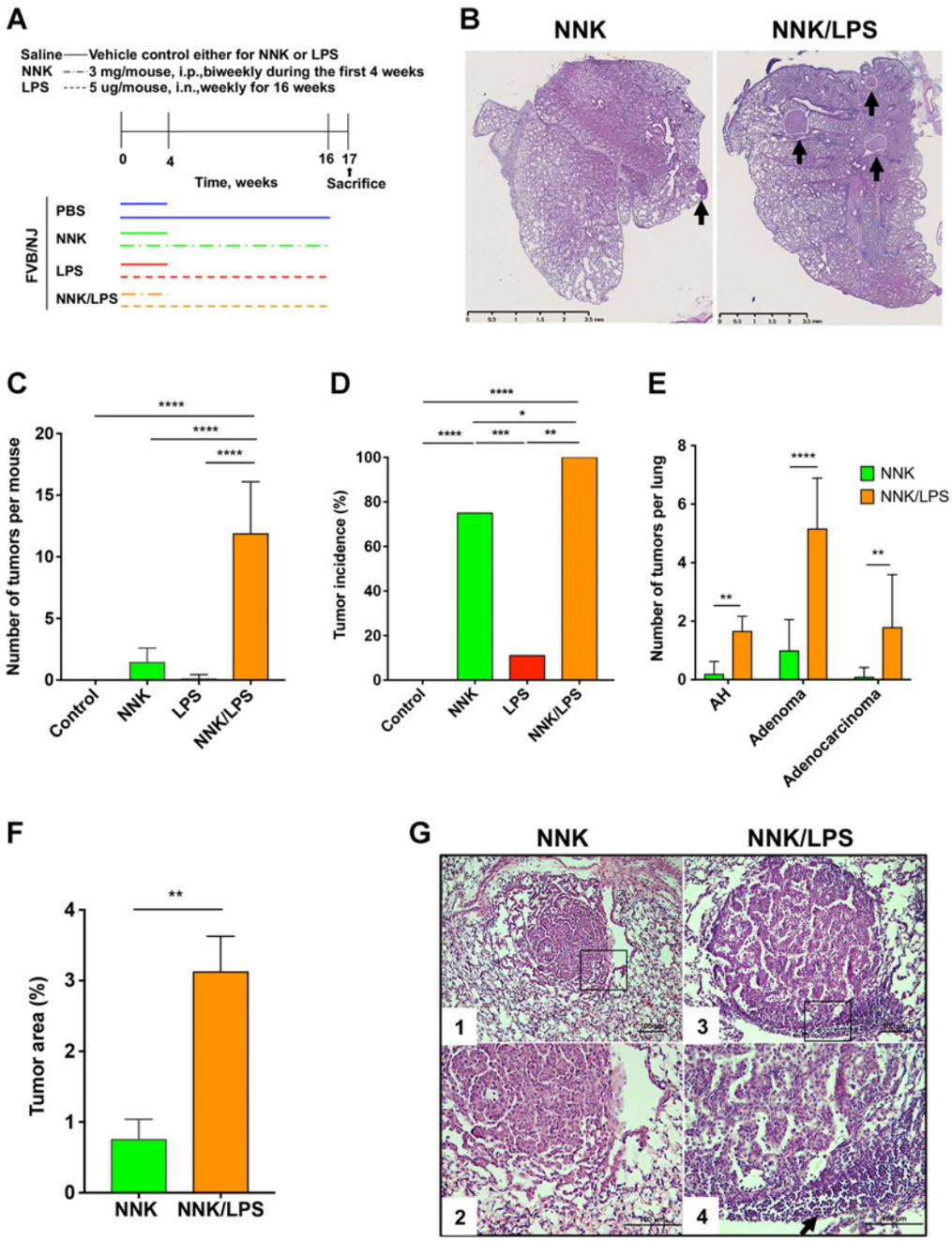

Figure 1.

Recurrent exposure to LPS promotes tobacco smoke carcinogen–induced lung tumorigenesis. **A,** FVB/NJ (7 weeks, female) mice were exposed with PBS, NNK (3 mg i.p. biweekly for 4 weeks), LPS (5 μg weekly i.n. instillation for 16 weeks), or NNK and LPS (NNK/LPS) combined. **B,** Hematoxylin and eosin staining of the tumor-bearing lungs. Arrows, lung tumors. **C,** Quantification of the number of tumors in mice exposed to PBS ($n = 5$), NNK ($n = 15$), LPS ($n = 9$), or NNK/LPS ($n = 11$). Results are mean ± SD of one representative dataset of four independent experiments. ****, $P < 0.0001$ using one-way ANOVA with *post-hoc* Bonferroni correction. **D,** Tumor incidence rate (percent) in various exposure groups. *, $P < 0.05$; **, $P < 0.01$; ***, $P < 0.001$; ****, $P < 0.0001$ using χ^2 test. **E,** The number of AH foci, adenomas, and adenocarcinomas in the lungs of NNK compared with NNK/LPS exposure mice. Values are mean ± SD. **, $P < 0.01$; ****, $P < 0.0001$ using two-way ANOVA with *post-hoc* Bonferroni correction. **F,** Tumor area (percent) was calculated in NNK ($n = 5$) and NNK/LPS exposure ($n = 5$). Values are mean ± SD. **, $P < 0.01$ using Student *t* test. **G,** Hematoxylin and eosin staining of tumors derived from NNK- and NNK/LPS-treated mice. Bottom, high-magnification images. Arrow, TILs. Scale bars, 100 μm.

Published OnlineFirst October 29, 2020; DOI: 10.1158/0008-5472.CAN-20-1994

Results

NNK-induced lung tumorigenesis is augmented by LPS-mediated chronic inflammation

To investigate the mechanism by which LPS-mediated chronic inflammation influences NNK-induced lung tumorigenesis, we employed a murine lung cancer model that combined NNK exposure with recurring intranasal LPS instillation (NNK/LPS; **Fig. 1A**). Lung tumors in mice treated with NNK alone were smaller and less frequent than tumors in mice treated with combined NNK/LPS (**Fig. 1B**). Quantitatively, mice treated with NNK alone had approximately 1.5 tumors per mouse, whereas mice exposed to LPS alone had no lung tumors (except one tumor in all LPS-treated mice; **Fig. 1C**). Combined NNK/LPS exposure increased lung tumors by 8-fold (**Fig. 1C**). In lung tumor incidence, tumors developed in approximately 75% NNK-exposed mice, whereas lung tumors developed in 100% NNK/LPS-exposed mice (**Fig. 1D**). Pathologic stage of proliferative pulmonary lesions including alveolar hyperplasia (AH), adenoma, and adenocarcinoma (**Fig. 1E**; Supplementary Fig. S2) as well as tumor area (**Fig. 1F**) were greater in the combined NNK/LPS mice compared with the NNK alone mice. Notably, NNK-induced lung tumors displayed limited inflammatory cells infiltrates (**Fig. 1G**, plots 1 and 2). In contrast, tumors in combined NNK/LPS-treated mice displayed enhanced inflammatory cell recruitment with infiltrating leukocytes adjacent to and throughout the tumors (**Fig. 1G**, plots 3 and 4, arrow). These results suggested recurrent LPS exposure augmented NNK-induced lung tumorigenesis by recruiting tumor-infiltrating leukocytes in the tumor microenvironment.

Combined NNK/LPS exposure alters lung inflammatory profiles and increases the accumulation of immunosuppressive cells

To assess the consequences of LPS-mediated inflammation in the lung, we analyzed the cellular profiles and cytokines in the bronchoalveolar lavage (BAL). Total and differential BAL leukocytes were not different between control and NNK-treated mice (**Fig. 2A** and **B**). However, total and differential BAL leukocytes including macrophages, neutrophils, and lymphocytes increased in the presence of chronic LPS exposure regardless of NNK treatment (**Fig. 2A** and **B**). Similarly, BAL cytokines were not different between control and NNK-exposed mice, whereas IP-10, IL17, G-CSF, KC, and MIP-1α increased in the LPS exposure group (**Fig. 2C–G**). Notably, combined NNK/LPS exposure further increased the inflammatory cytokines IL17, G-CSF, KC, and MIP-1α (**Fig. 2D–G**), which is indicative of granulocytic MDSC recruitment and development, and the formation of immunosuppressive microenvironment (28, 29).

To further characterize immune cells in the tumor-bearing mice, we performed the immune cell profiling of lung tissue by flow cytometry. The number of $CD4^+$ T-helper cells (Th1, Th17), $CD8^+$ T-cytotoxic cells (Tc1), Tregs, granulocytic MDSCs (Gr-MDSCs), and monocytic MDSCs (M-MDSCs) did not differ between NNK-exposed and control mice (**Fig. 2H–M**). In contrast, the combined NNK/LPS group had increased Th1, Th17, Tregs, and MDSCs as compared with all other exposure groups (**Fig. 2H–L**). Tc1 cells did not differ among any treatment groups (**Fig. 2M**). Our data indicated that combined NNK/LPS exposure increased lung inflammatory cytokine production and recruitment of immunosuppressive cells (i.e., MDSCs and Tregs) in the tumor microenvironment.

Recurrent LPS exposure enriches T-cell–related immune response pathways and induces T-cell exhaustion

To elucidate the regulatory mechanisms and gene signatures of NNK/LPS-mediated inflammatory cytokines and immunosuppressive cellular phenotypes, we performed the mRNA microarray analysis of mouse lungs from the four experimental conditions. Unsupervised hierarchical clustering of 1,179 DEGs identified by comparing NNK/LPS versus NNK yielded 2 main clusters, which separated control and NNK group from LPS and NNK/LPS group (**Fig. 3A**, left plot). We identified a cluster enriched in lymphocyte chemokines (*Cxcl9, Cxcl10, Cxcl13*, and *Ccl20*) and inhibitory checkpoint receptor (*Pdcd1*) that increased following recurrent LPS exposure (**Fig. 3A**, left plot, between 2 black lines, and right plot). We also analyzed the 1,179 DEGs using Ingenuity Pathway Analysis (IPA, RRID:SCR_008653), and the results suggested that multiple enriched pathways are associated with T-cell immune responses (**Fig. 3B**; Supplementary Table S3). These results were further validated by qRT-PCR for checkpoint inhibitory receptor transcripts, including *Pdcd1, Ctla4, Lag3*, and *Tim-3* (Supplementary Table S4), which increased in the presence of recurrent LPS exposure in both LPS and NNK/LPS groups (**Fig. 3C**). Importantly, *Pdcd1* transcripts increased more in the NNK/LPS group as compared with other inhibitory checkpoint receptor transcripts *Ctla4, Lag3*, and *Tim3* (**Fig. 3C**). Taken together, T-cell–related immune response and associated T-cell exhaustion pathways were enriched in transcripts in the recurrent LPS exposure groups.

Combined NNK/LPS exposure augments PD-1/programmed cell death ligand-1 axis in the tumor microenvironment

To characterize the tumor-infiltrating T lymphocytes (TIL) and PD-1 expression in the tumor microenvironment, we performed multiplex IHC staining of CD4, CD8, and PD-1 to examine the TILs and PD-1 expression in the tumor microenvironment (**Fig. 4A**). $CD4^+$ and $CD8^+$ T cells and $PD\text{-}1^+$ cells increased in lung tumors of NNK/LPS group compared with NNK group (**Fig. 4A**). PD-1 expression was frequently colocalized with tumor-infiltrating $CD4^+$ and $CD8^+$ T cells, especially in NNK/LPS-treated lung tumors (**Fig. 4A**, bottom plots). The number of tumor-infiltrating $CD4^+$ and $CD8^+$ cells of NNK/LPS group was greater than that of NNK group. (**Fig. 4B**, left plot). Also, the percentage of $CD4^+$ cells and $CD8^+$ cells colocalized with PD-1 protein was higher in NNK/LPS group than NNK group (**Fig. 4B**, right plot). Furthermore, we confirmed that the ligand of PD-1 protein, programmed cell death ligand-1 (PD-L1), expression was increased in mouse lung protein (**Fig. 4C**) and in IHC-stained sections of NNK/LPS group as compared with that of NNK group (**Fig. 4D**). Collectively, recurrent LPS exposure increased tumor-infiltrating T cells with colocalized PD-1 expression and tumor PD-L1 expression in NNK-induced lung tumors.

Antitumor efficacy by PD-1 blockade antibody is affected by LPS-mediated inflammatory responses

Based on the increased PD-1/PD-L1 protein in tumors induced by NNK/LPS exposure, we hypothesized that PD-1 checkpoint inhibition by anti–PD-1 antibody could inhibit inflammation-promoted lung tumorigenesis. We first evaluated the anti–PD-1 antibody treatment after combined 4-week NNK and 10-week LPS exposure when lung tumors formation is at an early stage (**Fig. 5A** and **B**). Extending LPS exposure to 16 weeks (**Fig. 5** and **D**) increased lung tumor number as compared with 10 weeks in NNK/LPS-exposed mice (13.6 vs. 9.8, $P = 0.0025$, **Fig. 5B** and **D**). Anti–PD-1 treatment effectively decreased lung tumors in the NNK/LPS group, but did not differ in the NNK

Published OnlineFirst October 29, 2020; DOI: 10.1158/0008-5472.CAN-20-1994

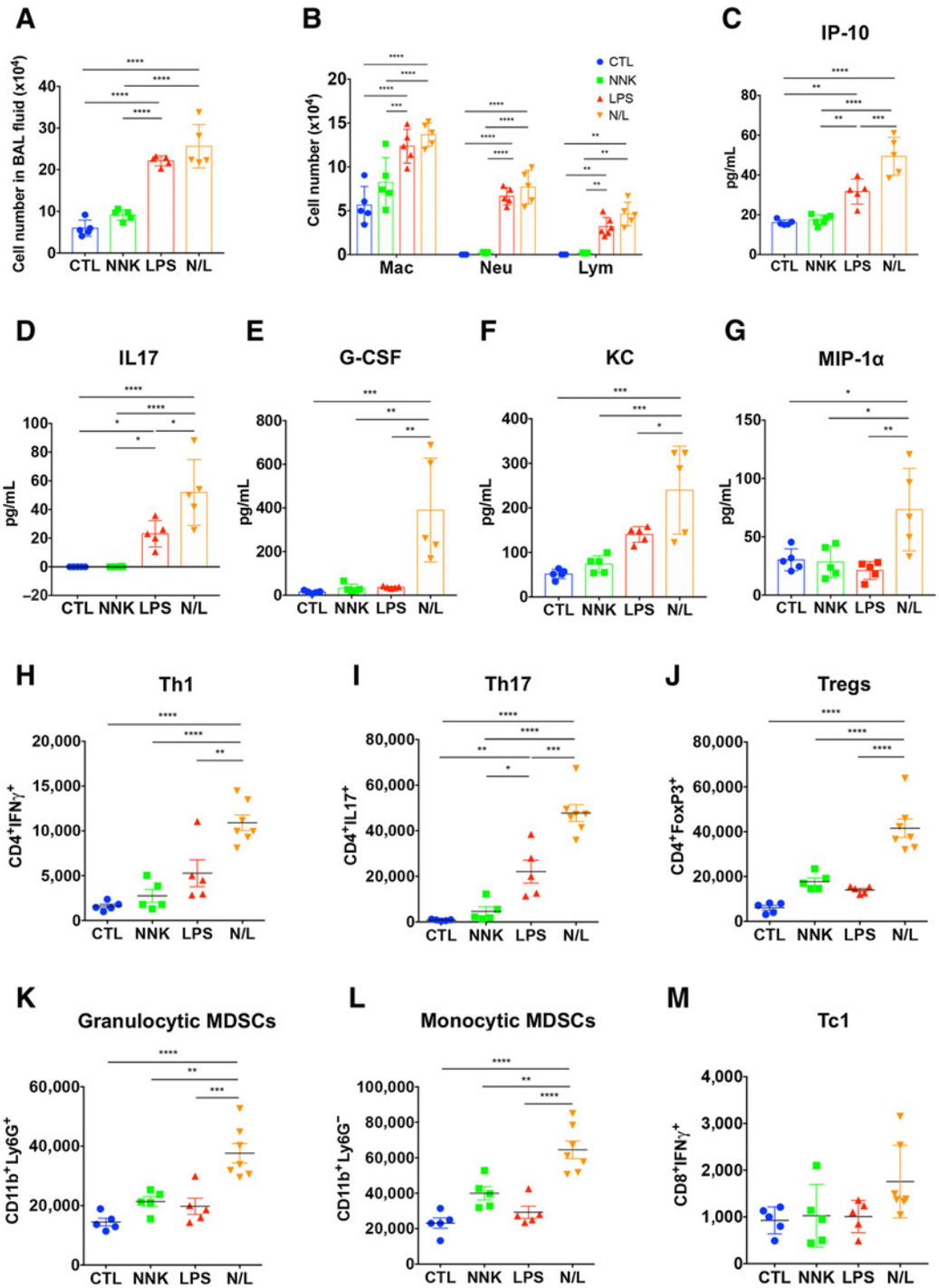

Figure 2.

LPS alters tobacco smoke carcinogen–induced inflammatory profiles and increased the accumulation of immunosuppressive cells in the lungs. **A,** FVB/NJ (7 weeks, female) mice were exposed with PBS, NNK (3 mg i.p. biweekly for 4 weeks), LPS (5 μg weekly i.n. instillation for 16 weeks), or NNK and LPS (NNK/LPS) combined. Quantification of total cell number from BAL of exposure groups ($n = 5$ for each group). **B,** Differential cell counts of inflammatory cells in BAL fluid. **C–G,** Cytokines/chemokines in BAL and protein extracts ($n = 5$ for each group) of exposure groups were analyzed by Luminex assay and enzyme-linked immunosorbent assay. Flow cytometry analysis of immune cell population of mouse lungs in different exposure groups harvested at week 17 after initiation of NNK and LPS treatment as indicated in **Fig. 1A**. The cellular markers included Th1 (**H**), Th17 (**I**), Tregs (**J**), granulocytic MDSCs (**K**), monocytic MDSCs (**L**), and Tc1 (**M**). Values are mean ± SD and are representative of three independent experiments. *, $P < 0.05$; **, $P < 0.01$; ***, $P < 0.001$; ****, $P < 0.0001$ using one-way ANOVA with *post-hoc* Bonferroni correction. CTL, control; Th1, T-helper cell type 1; Th17, T-helper cell type 17; Tc1, $CD8^+$ cytotoxic T lymphocyte.

Published OnlineFirst October 29, 2020; DOI: 10.1158/0008-5472.CAN-20-1994

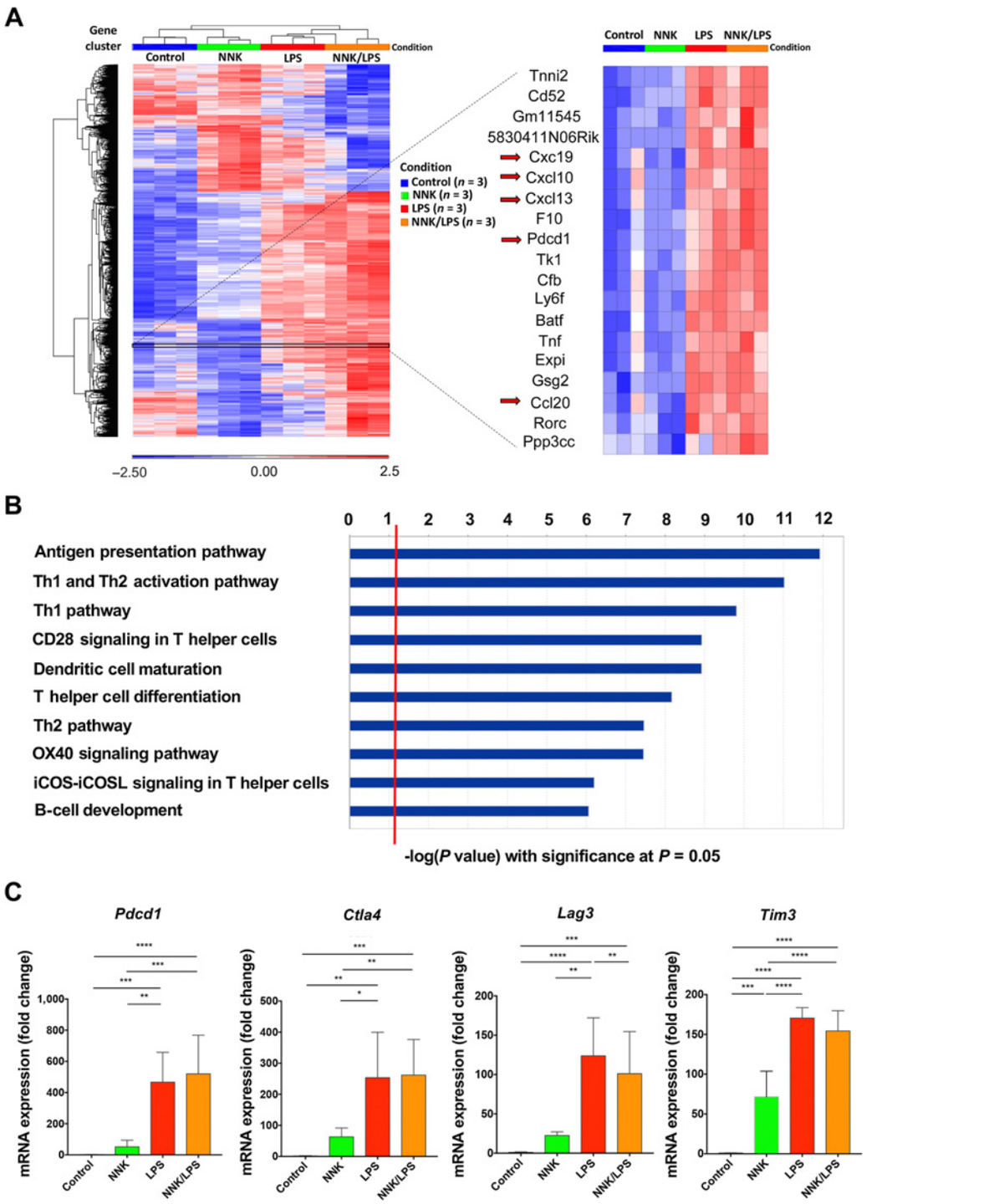

Figure 3.

LPS-mediated chronic inflammation increased cell-related immunity and induces T-cell exhaustion. FVB/NJ (7 weeks, female) mice were exposed with PBS, NNK (3 mg i.p. biweekly for 4 weeks), LPS (5 μg weekly i.n. instillation for 16 weeks), or NNK and LPS (NNK/LPS) combined. Mouse lung mRNA was analyzed by microarray ($n = 3$ for each group). **A,** Unsupervised hierarchical clustering heatmap based on the DEGs ($n = 1{,}179$, absolute fold change ≥ 2, FDR < 0.05) between NNK/LPS and NNK. Arrows indicate lymphocyte recruitment CXCL9, CXCL10, CXCL13, and CCL20, and inhibitory checkpoint receptor PDCD1 transcripts. **B,** Pathways identified by IPA based on 1,179 DEGs. **C,** Levels of inhibitory checkpoint receptors, PDPD1, CTLA-4, LAG3, and TIM-3 in each exposure group were quantified by quantitative real-time PCR ($n = 6$/group). Values are mean ± SD. **, $P < 0.01$; ***, $P < 0.001$; ****, $P < 0.0001$ using one-way ANOVA with *post-hoc* Bonferroni correction. CCL20, chemokine (C-C motif) ligand 20; CTLA-4, cytotoxic T-lymphocyte associated protein 4; CXCL9, chemokine (C-X-C motif) ligand 9; CXCL10, chemokine (C-X-C motif) ligand 10; CXCL13, chemokine (C-X-C motif) ligand 13; LAG3, lymphocyte-activation gene 3; PDCD1, programmed cell death 1; TIM-3, T-cell immunoglobulin mucin-3.

Published OnlineFirst October 29, 2020; DOI: 10.1158/0008-5472.CAN-20-1994

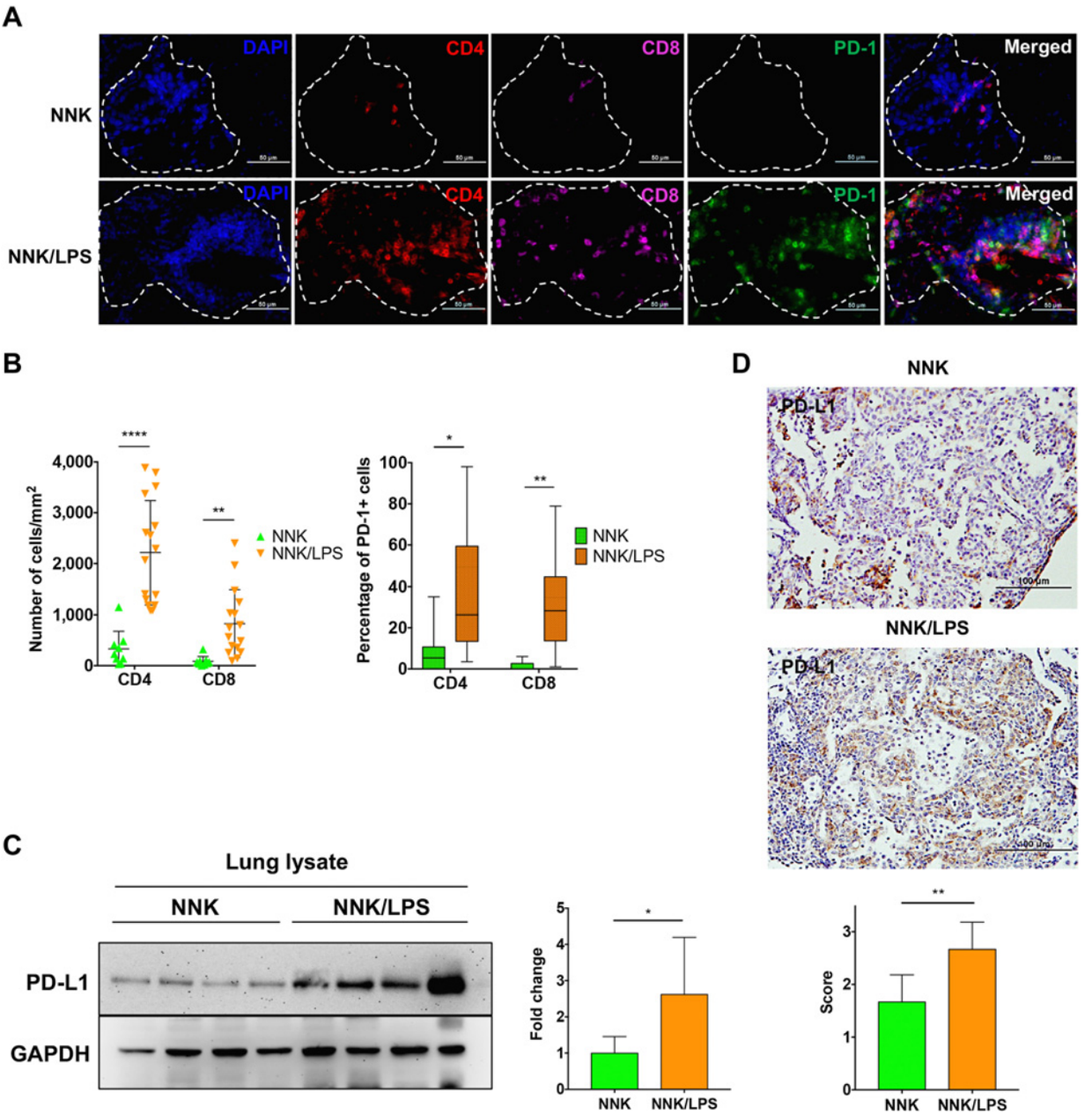

Figure 4.

Combined NNK and LPS exposure increases TILs with colocalized PD-1 and increases tumor PD-L1 expression. **A,** Representative CD4 (red), CD8 (magenta), and PD-1 (green) cell infiltration in lung tumors. Nuclei are identified by DAPI staining. Scale bars, 50 μm. Dotted lines outline tumor boundaries. **B,** Quantification of $CD4^+$ and $CD8^+$ TILs and percentage of PD-1 expression in $CD4^+$ and $CD8^+$ TILs. *, $P < 0.05$; **, $P < 0.01$; ****, $P < 0.0001$ using Student *t* test. **C,** PD-L1 levels in lung lysates from NNK ($n = 4$) and NNK/LPS-treated mice ($n = 4$), representative results from one experiment of three individual experiments. *, $P < 0.05$ using Mann–Whitney test. **D,** Representative PD-L1 IHC staining of NNK and LPS/NNK-exposed lung tumors, and the positive tumor cell surface staining was scored. Scale bars, 100 μm. DAPI, 4′,6-diamidino-2-phenylindole.

group (**Fig. 5B**). Interestingly, when LPS instillation was extended from 10 to 16 weeks (**Fig. 5C**), the anti–PD-1 treatment only slightly decreased lung tumors and did not reach the statistical significance, suggesting that prolonged/persistent LPS treatment induced additional inhibitory mechanisms in the tumor microenvironment (**Fig. 5D**).

Based on our findings that MDSCs increased and chemokines/cytokines profiles altered in the tumor microenvironment after 16-week combined NNK/LPS exposure (**Fig. 2**), we hypothesized that infiltrating MDSCs contribute to this inhibitory activity. Anti-Ly6G antibody, which depletes Gr-MDSCs, decreased lung tumor number compared with isotype control, indicating a tumor-promoting effect

Published OnlineFirst October 29, 2020; DOI: 10.1158/0008-5472.CAN-20-1994

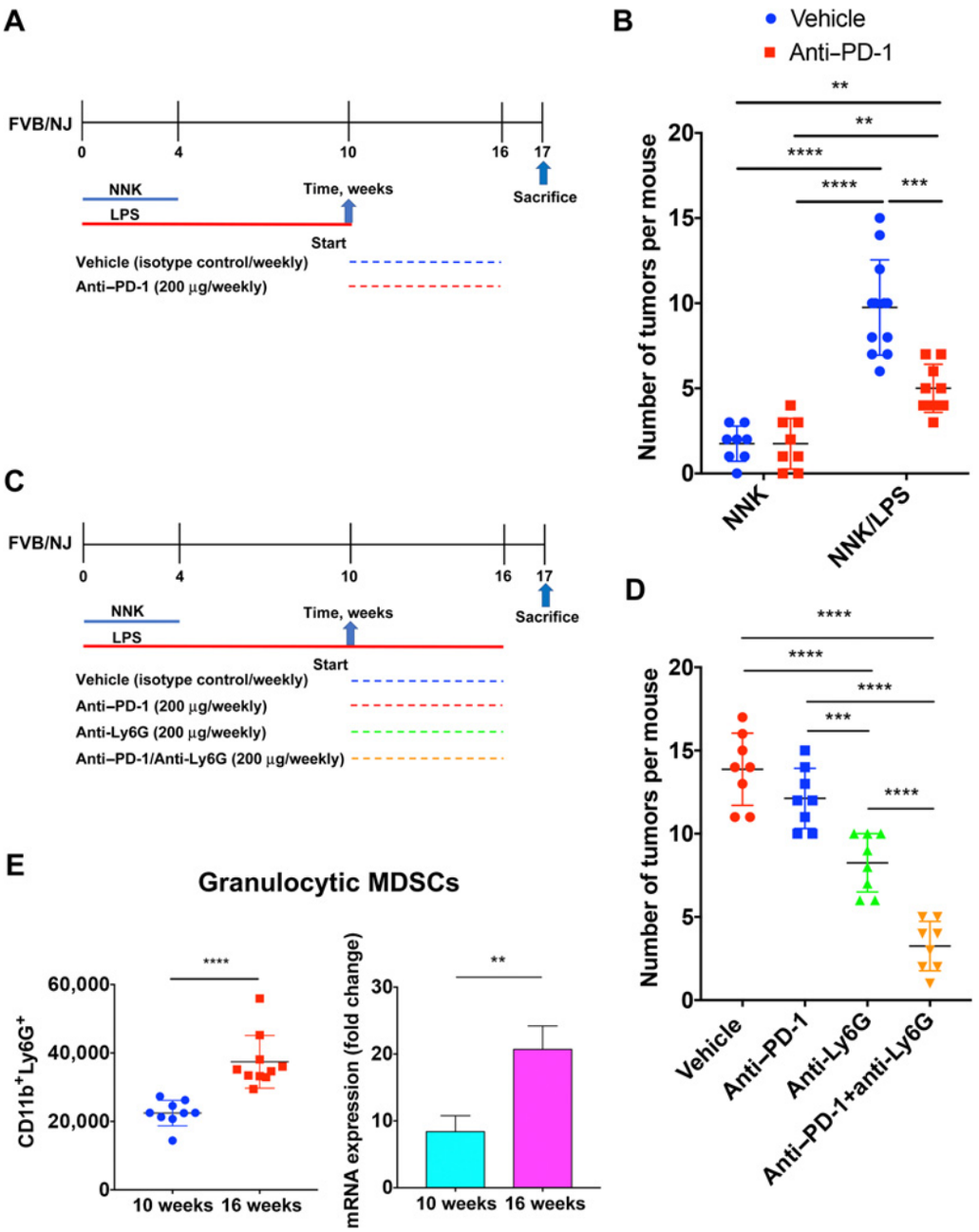

Figure 5.

LPS-mediated inflammation alters immune contexture and correlates with PD-1 blockade efficacy. **A,** The treatment paradigm of anti–PD-1. Mice were exposed to NNK or NNK combined with 10-week LPS exposure and treated with either IgG control (IgG2a) or anti–PD-1 for 6 weeks. **B,** After treatments from weeks 10 to 16 without additional LPS exposure, anti–PD-1 treatment decreased lung tumor number in NNK/LPS mice but did not differ in NNK mice as compared with IgG2a control mice. **, $P < 0.01$; ***, $P < 0.001$ using Student *t* test. **C,** The treatment paradigm of anti–PD-1 and anti-Ly6G. Mice were exposed to NNK combined with 16-week LPS treated for either IgG control ($n = 8$), anti–PD-1 ($n = 8$), anti-Ly6G ($n = 8$), or combined anti–PD-1 and anti-Ly6G ($n = 8$) for 6 weeks. **D,** After 16 weeks, anti–PD-1 treatment only slightly decreased lung tumors in NNK/LPS mice and was not statistically significant as compared with IgG2a control. Anti-Ly6G antibody effectively inhibited NNK/LPS-induced lung tumors and further enhanced treatment efficacy in combination with ant–PD-1 antibody. Values are mean ± SD and are representative of two independent experiments. ***, $P < 0.001$; ****, $P < 0.0001$ using one-way ANOVA with *post-hoc* Bonferroni correction. **E,** Flow cytometry analysis of granulocytic MDSCs of mouse lungs in 10-week and 16-week NNK/LPS group ($n = 10$ for each group). Values are mean ± SD. ****, $P < 0.0001$ using Student *t* test. The granulocytic MDSC signature of the 10-week and 16-week NNK/LPS group in the mouse microarray dataset was analyzed. Values are mean ± SD. **, $P < 0.01$ using Mann–Whitney test. IgG, immunoglobulin G; Ly6G, lymphocyte antigen 6 G.

Published OnlineFirst October 29, 2020; DOI: 10.1158/0008-5472.CAN-20-1994

by Gr-MDSCs (**Fig. 5D**). Importantly, treatment with combined anti–PD-1 and anti-Ly6G antibodies further decreased lung tumor number compared with the anti–PD-1 or anti-Ly6G treatment alone, suggesting enhanced antitumor activity by the combinatory treatment (**Fig. 5D**). In addition, we confirmed that infiltrating Gr-MDSCs increased in the tumor-bearing mouse lungs when LPS exposure was extended from 10 to 16 weeks in the NNK/LPS combined exposure (**Fig. 5E**, left plot). Consistent with the flow cytometry data, Gr-MDSC gene signature transcripts increased more at 16 weeks than at 10 weeks of NNK/LPS exposure (**Fig. 5E**, right plot). In addition, T-cell, B-cell, Th17-cell, and NK-cell signature transcripts increased more at 16 weeks than at 10 weeks of NNK/LPS exposure (Supplementary Fig. S3), suggesting that the less prominent antitumor effect of anti–PD-1 antibody was not due to decreased adapted cellular immune components. Our results indicate that PD-1 blockade effectively inhibited inflammation-associated lung tumorigenesis in NNK-treated mice combined with a shorter 10-week LPS exposure. For lung tumors resulting from extended exposure of 16-week NNK/LPS exposure, immunotherapy that combined PD-1 blockade with Gr-MDSC depletion significantly inhibited tumor growth and enhanced the treatment efficacy.

Immune gene signature reveals PD-1 blockade responsiveness and progression-free survival in patients with NSCLC

Our results demonstrated that immune contexture in the tumor microenvironment could affect PD-1 blockade efficacy. Thus, we hypothesized that the expression of a unique immune gene signature in the tumor microenvironment could reveal PD-1 blockade treatment responsiveness. To test this hypothesis, we analyzed transcriptomes from a cohort of 35 NSCLC patients with varied PD-1 blockade response (GSE93157; Supplementary Table S1; ref. 15). We identified a 130-gene immune gene panel from the cohort and established immune cell gene signatures for T cell, B cell, NK cell, and Th17 cell based on curated data from eight publicly available expression datasets (Supplemental Table S2; ref. 13). We applied this gene set to the cohort of patients with NSCLC, and separated patients as NPD, including CR, PR, and SD patients, versus the patients with PD. We generated 4 hierarchical DEGs clusters (C1–C4, leftmost column) based on the supervised patient groups (**Fig. 6A**). Overall, the transcriptomes of patients with NPD displayed an increased expression of immune-related genes compared with those of patients with PD. Most T-cell– and B-cell–associated markers localized to the C1 cluster, whereas NK-cell, Th17-cell, and other immune-related makers were observed in the other clusters (**Fig. 6A**). Moreover, T-cell, B-cell, Th17-cell, and NK-cell signatures exhibited higher expression in patients with NPD than PD (**Fig. 6B**). ROC analysis was performed to evaluate the diagnostic accuracy of these gene signatures to predict treatment responses (NPD vs. PD) in GSE93157. The results indicated excellent diagnostic accuracy for which all immune cell signatures were with an area under curve > 0.7 and $P < 0.05$ (Supplementary Fig. S4A–S4E). In addition, the increased expression of immune cell gene signature was associated with prolonged progression-free survival in patients with both squamous and nonsquamous NSCLC (**Fig. 6C**).

Comparison of the immune gene signature of NSCLC patients with PD-1 blockade responsiveness to the immune gene signature in the murine tumor model

Next, we examined the possible utility of our inflammation-associated murine lung cancer model in recapitulating patients with NSCLC receiving immunotherapy treated with PD-1 blockade. We found that 127 mouse homologous genes corresponded with a 130-gene human immune gene panel from the GSE93157 cohort. Using these 127 genes, we performed immune gene signature analysis of the mouse mRNA microarray dataset. The supervised hierarchical clustering revealed 3 gene clusters (C1–C3, leftmost column) with similar immune cell gene signatures identified for the same types of cells in the human lung cancer cohort (**Fig. 7A**). The immune cell gene signatures for T cell, B cell, Th17 cell, and NK cell represented stepwise-induced innate and adaptive immune responses, which had increased expression in the NNK/LPS group as compared with NNK group (**Fig. 7B**). Collectively, these findings support that our NNK/LPS lung tumor model well represents the "hot" tumor microenvironment with profound infiltrating immune cell signatures observed in the human lung cancer dataset.

Discussion

In this study, we characterized a two-staged murine lung cancer model, in which a tobacco smoke–associated carcinogen, NNK, initiates lung tumorigenesis, which is augmented through LPS-mediated chronic inflammation that, in turn, leads to an immunosuppressive tumor microenvironment. This inflammation-associated lung cancer murine model was originally established by our laboratory to evaluate the *Kras* mutation frequency under recurrent inflammation (17) and subsequently reproduced by other research groups (30, 31).

In this model, immunosuppression was demonstrated by MDSCs and Treg accumulation, induced T-cell exhaustion, and increased PD-1/PD-L1 checkpoint pathway activities. PD-1 blockade exhibited favorable efficacy during an early tumor-forming stage with a shorter LPS-induced inflammation. Moreover, a combined treatment of PD-1 blockade and MDSC depletion exhibited stronger antitumor activity. Our findings support the concept that a combined treatment of PD-1 blockade and MSDC depletion could be a novel therapeutic approach for treating lung cancers associated with chronic pulmonary inflammation, as are frequently present in COPD patients with recurrent infections. In addition, we identified an immune gene signature, which effectively predicted treatment responses and survival outcomes in patients with lung cancer received PD-1 blockade therapy.

Cigarette smoke–induced airway inflammation plays an essential role in the pathogenic process of COPD and lung cancer (32). It is characterized by increased numbers of neutrophils together with increased macrophage and T lymphocytes in peripheral airways, lung parenchyma, and pulmonary vessels (33). One limitation of our study is that the COPD status of the patients with lung cancer in GSE93157 was not available. Approximately 40% to 70% of lung cancer cases have coexisting COPD (34). The majority of the GSE93157 cohort (92%) were current or former smokers that could have cigarette smoke–related pulmonary inflammation. These patients had increased cytokines and chemokines similar to patients with COPD (32). Previously, nebulized LPS has been reported to mimic the effects of cigarette smoke in the lower airway of laboratory animals and humans, resulting in bronchoalveolar neutrophil influx, airway obstruction, bronchial hyperresponsiveness, and pulmonary protein extravasation (35–38). These common features of pulmonary inflammation supported a link of this inflammation-associated murine lung cancer model with the human lung cancer cohort analyzed in this study.

Although several inflammation-associated lung cancer models have been established and studied, the effect of immune contexture during chronic inflammation on lung tumorigenesis and the efficacy of immune checkpoint inhibitors have not been defined in these models. Furthermore, some of the models are either genetically *Kras*-driven lung cancer models (39–41) or using susceptible strain such as A/J

Published OnlineFirst October 29, 2020; DOI: 10.1158/0008-5472.CAN-20-1994

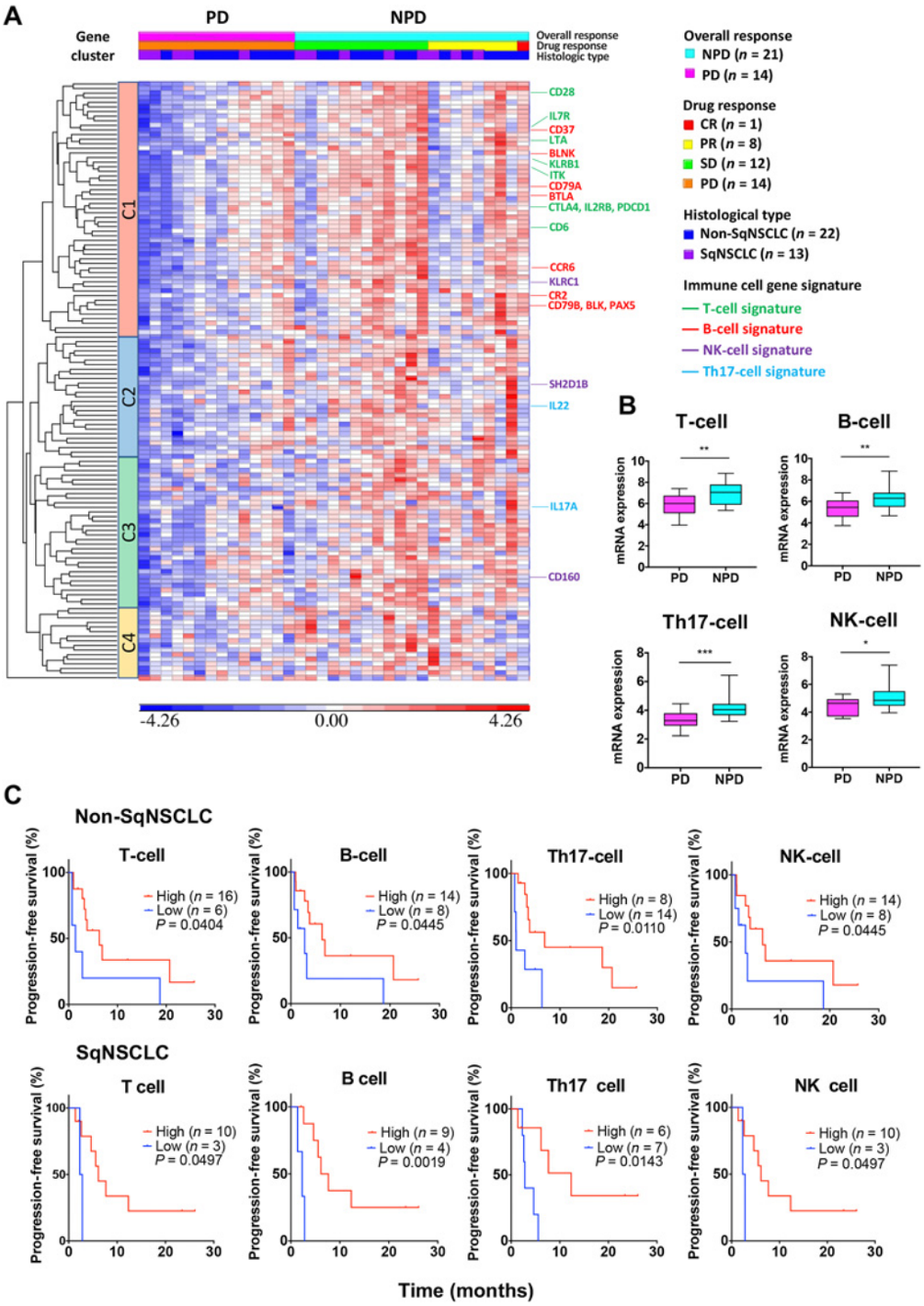

Figure 6.

Immune gene signatures predict responsiveness to PD-1 blockade and are associated with progression-free survival. Tumor samples of 35 patients with NSCLC before anti–PD-1 treatment were analyzed for the gene expression using the GSE93157 dataset. **A,** Expression profiles of 130 DEGs from NPD and PD tumors (red, increased; blue, decreased as compared with mean for each gene). Overall response (NPD and PD), drug response (CR, PR, SD, and PD), and histologic type (non-SqNSCLC and SqNSCLC) are indicated at the top of the heatmap. Immune cell gene signatures for T cell, B cell, Th17 cell, and NK cell are indicated. **B,** Gene signatures across patients with PD and NPD status. *, $P < 0.05$; **, $P < 0.01$; ***, $P < 0.001$ using Student *t* test. **C,** Kaplan–Meier survival analysis based on selected gene signatures in non-SqNSCLC and SqNSCLC. *P* value determined with log-rank test. Th17, T-helper cell type 17.

Published OnlineFirst October 29, 2020; DOI: 10.1158/0008-5472.CAN-20-1994

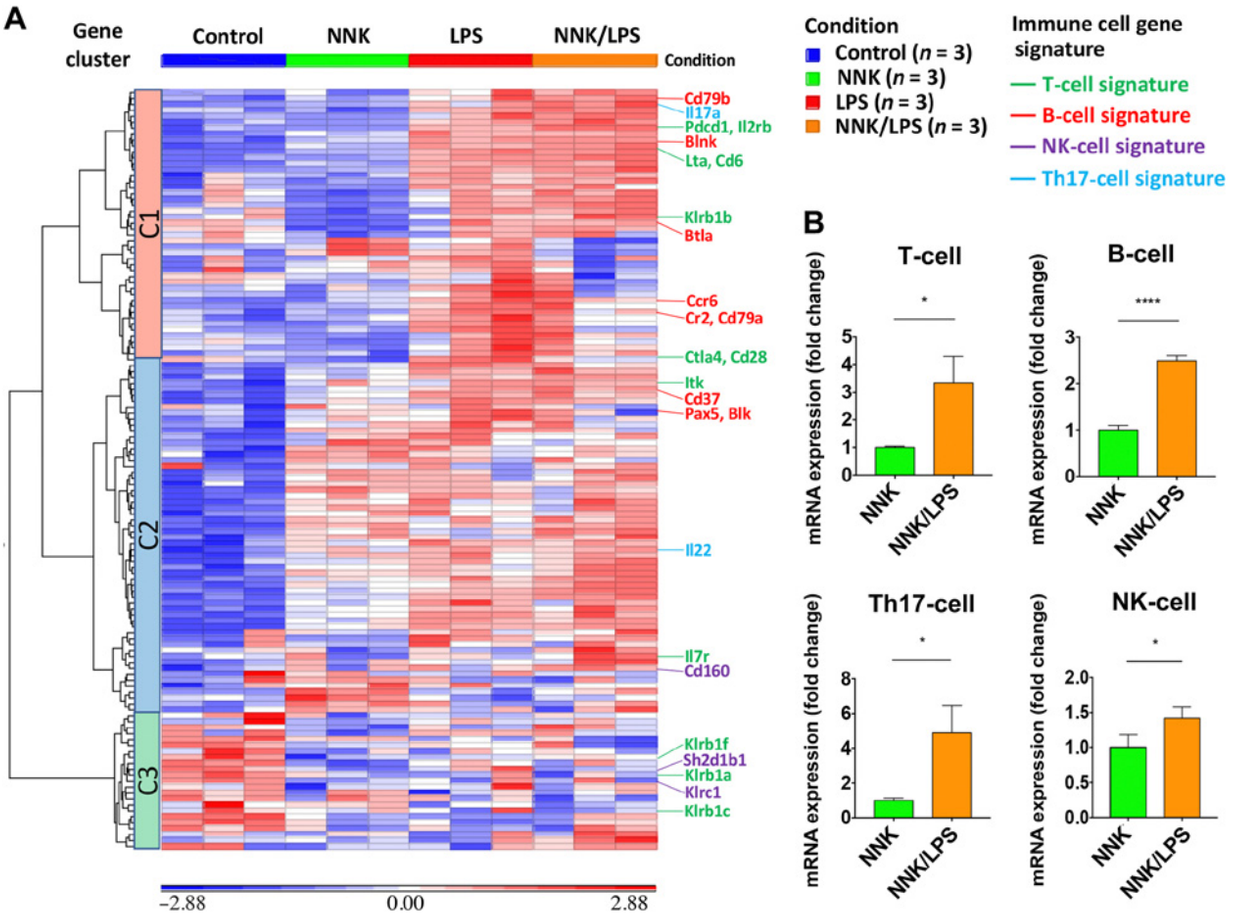

Figure 7.

Immune gene signatures demonstrate the clinical relevance of the mouse lung cancer model to patients with NSCLC. **A,** The immune gene profiling of mouse lungs after treatments of PBS, NNK, LPS, and NNK/LPS for 16 weeks. Mouse orthologs ($n = 127$ transcripts) were identified from the human immune gene panel ($n = 130$ transcripts) extracted from GSE93157 (Supplementary Table S2). The immune gene profiling of mouse lungs after treatments was presented by clustering heatmap (red, increased; blue, decreased as compared with mean for each gene). Immune cell gene signatures including T cell, B cell, Th17 cell, and NK cell were labeled. **B,** Immune cell gene signatures for T cell, B cell, Th17 cell, and NK cell were quantified. Values are mean ± SD. *, $P < 0.05$; ****, $P < 0.0001$ using Mann–Whitney test.

mice, which develop 88% to 100% *Kras* mutations in NNK-induced lung tumors (42, 43). Although models using A/J mice are useful to study lung tumorigenesis, they do not reflect the broad spectrum of mutations in human lung adenocarcinomas (44). The FVB/NJ mouse strain used in this study typically generates *Kras* mutation rates of approximately 45% in NNK-induced lung tumors (17), which is close to the frequency of 32% *KRAS* mutation rates in human lung adenocarcinoma (45). In addition, we have performed preliminary studies suggesting that tumors in our model have a low frequency of *Egfr* mutations. Thus, this model could provide a useful tool to investigate lung tumorigenesis related to these mutations.

Although NNK alone did not generate many lung tumors in FVB/NJ as compared with A/J mice, FVB/NJ mice proved to be useful in determining the role of inflammation in promoting lung tumorigenesis and the efficacy of immunotherapy. The lack of PD-1 blockade treatment efficacy against NNK-induced lung tumors could be due to "cold immune tumor" or "non-T cell-inflamed tumor," as we demonstrated in **Figs. 2** and **3**. In FVB/NJ mice treated with NNK alone, lung tumors had few tumor-infiltrating immune cells with minimal production of cytokines and chemokines in the microenvironment. These "cold immune tumors" may not unleash the pre-existing immunity to initiate effective antitumor immunity through anti–PD-1 treatment (46). In FVB/NJ mice treated with NNK and LPS, lung tumor number increased 8-fold, which is greater than the 1.5-fold increase of lung tumors in A/J strain (30). These findings suggest that FVB/NJ mice are more susceptible to inflammation-promoted lung tumorigenesis and could be a more relevant mouse model to study the response of immunotherapy in inflammation-associated lung cancer.

We compared the immune responses of the two mouse strains, FVB/NJ and A/J, after being exposed to combined NNK and LPS. We analyzed the DEGs and downstream pathways of our FVB/NJ dataset and that of A/J GSE64027 dataset (31). There are 362 overlapped DEGs (Supplementary Fig. S5A), which were enriched in T-cell–related signaling pathways (Supplementary Fig. S5B), indicating that chronic LPS exposure induced common T-cell–inflamed tumor microenvironment regardless of mouse strains. This result is consistent with the increased Tregs, PD-1^{+}CD4^{+}, and PD-1^{+}CD8^{+} T cells in A/J mice (47) as well as in the FVB/NJ mice (**Figs. 2J** and **4B**).

Published OnlineFirst October 29, 2020; DOI: 10.1158/0008-5472.CAN-20-1994

Furthermore, the distinct immune response pathways in FVB/NJ were mainly involved in innate immunity pathways such as Fcγ receptor–mediated phagocytosis, NK cell signaling, and the production of nitric oxide reactive oxygen species in macrophages (Supplementary Fig. S5C), which are consistent with the dominate immune responses mediated by MDSCs from the phagocyte and macrophage lineages. In contrast, A/J mice were prone to have an adaptive immune response as indicated by enrichment in pathways such as PKCθ signaling in T lymphocytes, OX40 signaling, and CD28 signaling in T helper cells (Supplementary Fig. S5D). These results reflect the divergence of immune response patterns among inbred mouse strains, which could partially represent the heterogeneity of genetic and immune background in human population.

In this model, recurrent LPS exposure leads to increased lymphocyte recruitment into the lung, with the greatest increase in T cells. Our results indicate that in the inflammatory tumor microenvironment, elevated cytokines and persistent T-cell receptor overstimulation could induce T-cell exhaustion in areas surrounding lung tumors (48). The increased $CD4^+$ and $CD8^+$ TILs colocalized with increased PD-1 expression in NNK/LPS-treated mice supported the existence of exhausted TILs. Interestingly, patients with NSCLC with coexisting COPD often develop increases in exhausted $CD4^+$and $CD8^+$ TILs with coexpression of PD-1, CTLA-4, LAG3, and TIM-3 (11). This suggested that chronic inflammation–mediated dysregulation of immune responses correlated with exhausted TILs. In addition, PD-L1 increased in lung tumors of NNK/LPS-treated mice compared with those of NNK-treated mice, which may represent a response to IFNγ secretion by TILs and LPS-induced TLR-4 signaling (49).

Several past studies have attempted to identify the gene signatures for immune cellular phenotypes (19, 21,22, 24). Each has detected various gene sets for the individual immune cell type, but only a few have identified overlapped genes. This presents a challenge as to what immune gene signatures should be used for the specific immune cell types. To present a viable solution to this problem, we analyzed the available datasets from eight publications and defined the immune cell gene signatures for T cell, B cell, and NK cell, using the gene sets in specific immune cell types presented in two or more studies among eight gene datasets. Furthermore, we performed immune gene signature analysis of the murine lung cancer model using the gene sets identified from the human lung cancers under anti–PD-1 treatment to evaluate the clinical relevance of animal studies. In the murine model, NNK/LPS-exposed mice had increased T-cell gene signature expression as compared with NNK-exposed mice with similar signature expression pattern in human lung tumors, which distinguished patients with NPD from patients with PD, indicating a T-cell inflamed tumor microenvironment (**Figs. 6B and 7B**).

Trujillo and colleagues previously reported that T-cell inflamed tumor microenvironment was associated with favorable efficacy of PD-1 blockade (50), which was consistent with better response in 10-week NNK/LPS-treated mice and patients with NPD under successful anti–PD-1 treatment in GSE93157 cohort (**Fig. 5B**). However, the efficacy of anti–PD-1 treatment was diminished in 16-week LPS exposure (**Fig. 5D**) due to increased late-stage influx of immunosuppressive cells, such as Gr-MDSC in the tumor microenvironment (**Fig. 5E**). This occurred despite an appearance of an increased T-cell signature in 16-week NNK/LPS tumors as compared with 10-week NNK/LPS tumors (Supplementary Fig. S3). This reflects the complexity of immunologically "hot" tumors with various dynamics of infiltrating immune cells including immunosuppressive cells, which impair checkpoint inhibitor–mediated antitumor activity (46). These *in vivo* results provided a plausible explanation why that a subset of patients still had disease progression after anti–PD-1 treatment, despite high immune gene signature expression as seen in GSE93157 cohort (**Fig. 6A**). Furthermore, most T-cell and B-cell signature transcripts clustered together in both murine model and the lung cancer cohort with similar treatment responses and survival outcomes, suggesting the potential antitumor immunity of B cells and the possible B–T-cell interaction of antigen presentation, or antibody-mediated activities in the tumor microenvironment (24).

An immunosuppressive tumor microenvironment hinders natural host immune responses and the efficacy of cancer immunotherapies. MDSCs in the tumor microenvironment not only inhibit effector T-cell and NK-cell functions but also can directly promote tumor progression and metastasis (51). The percentage of myeloid cells increased in NNK/LPS mice including $CD11b^+Ly6G^+$ cells (Gr-MDSCs) and $CD11b^+Ly6G^-$ cells (M-MDSCs and other myeloid cells; ref. 52). After 16-week NNK/LPS exposure, multiple inflammatory cells increased in the tumor, especially Gr-MDSCs (**Fig. 2L**), which suppressed and impaired anti–PD-1 treatment efficacy (**Fig. 5D**). Gr-MDSCs' mediated immunosuppression and impaired anti–PD-1 treatment efficacy have been observed in studies of other cancer types (52–54).

Our findings demonstrated that Gr-MDSC depletion significantly decreased lung tumors, and with combined anti–PD-1 further enhanced antitumor response (**Fig. 5D**). In a related study, Clavijo and colleagues reported that Gr-MDSC depletion in mice enhanced effector immune cell ($CD8^+$ TIL $CD107a^+$ and NK $CD107a^+$) activation and rescued antigen-specific T-lymphocyte reactivity lost during tumor progression in oral cancer (53). In agreement with our result, Gr-MDSC depletion within a T-cell inflamed syngeneic system sensitized tumors to anti–CTLA-4 antibody-induced tumor rejection. These results suggest outcomes could be improved by identifying the coexistence of the inhibitory signals, such as the presence of immunosuppressive cells (e.g., MDSCs and Tregs). Therefore, removal of these inhibitory signals, such as MDSC depletion together with checkpoint inhibitors, could improve cancer immunotherapy efficacy.

Our current study represents a clinically relevant murine lung cancer model, similar to those COPD-like airway inflammation promoted lung cancer development with the characteristics of a favorable immunosuppressive microenvironment for tumor progression. Furthermore, the LPS-mediated inflammatory microenvironment affects PD-1 blockade efficacy, and combined PD-1 blockade and MDSC depletion improved treatment efficacy. Finally, we have identified valuable immune gene signatures associated with treatment responses and survival outcome in patients with NSCLC under immunotherapy. This preclinical model and the immune gene signatures could be potentially useful for the further exploration and evaluation of immune checkpoint inhibitors for NSCLC treatment.

Authors' Disclosures

No disclosures were reported.

Authors' Contributions

C.-H. Liu: Conceptualization, data curation, software, formal analysis, validation, investigation, visualization, methodology, writing-original draft, project administration, writing-review and editing. **Z. Chen:** Conceptualization, data curation, supervision, investigation, visualization, writing-original draft, writing-review and editing. **K. Chen:** Data curation, investigation. **F.-T. Liao:** Data curation, formal analysis. **C.-E. Chung:** Data curation, investigation. **X. Liu:** Data curation. **Y.-C. Lin:** Data curation. **P. Keohavong:** Conceptualization, resources. **G.D. Leikauf:** Writing-review and editing. **Y.P. Di:** Conceptualization, resources,

data curation, supervision, funding acquisition, investigation, methodology, project administration, writing-review and editing.

Acknowledgments

Funding for this work was provided by NIH (R01HL125128 and R01AI133351) and Intramural Research Program of the NIH (NIDCD: ZIA-DC-000016, ZIA-DC-000073, ZIA-DC-000074). We thank Drs. Clint Allen and Nicole Schmitt in the Head and Neck Surgery Branch, National Institute on Deafness and Other Communication Disorders, NIH, for their helpful comments and suggestions. We acknowledge the use of the PartekGS software licensed through the Molecular Biology Information Service of the Health Sciences Library System at the University of Pittsburgh.

The costs of publication of this article were defrayed in part by the payment of page charges. This article must therefore be hereby marked *advertisement* in accordance with 18 U.S.C. Section 1734 solely to indicate this fact.

Received June 15, 2020; revised September 10, 2020; accepted October 26, 2020; published first October 29, 2020.

References

1. Siegel RL, Miller KD, Jemal A. Cancer statistics, 2019. CA Cancer J Clin 2019;69:7–34.
2. Molina JR, Yang P, Cassivi SD, Schild SE, Adjei AA. Non-small cell lung cancer: epidemiology, risk factors, treatment, and survivorship. Mayo Clin Proc 2008;83:584–94.
3. Malhotra J, Malvezzi M, Negri E, La Vecchia C, Boffetta P. Risk factors for lung cancer worldwide. Eur Respir J 2016;48:889–902.
4. Desai H, Eschberger K, Wrona C, Grove L, Agrawal A, Grant B, et al. Bacterial colonization increases daily symptoms in patients with chronic obstructive pulmonary disease. Ann Am Thorac Soc 2014;11:303–9.
5. Crusz SM, Balkwill FR. Inflammation and cancer: advances and new agents. Nat Rev Clin Oncol 2015;12:584–96.
6. Wang D, DuBois RN. Immunosuppression associated with chronic inflammation in the tumor microenvironment. Carcinogenesis 2015;36:1085–93.
7. Diakos CI, Charles KA, McMillan DC, Clarke SJ. Cancer-related inflammation and treatment effectiveness. Lancet Oncol 2014;15:e493–503.
8. Borghaei H, Paz-Ares L, Horn L, Spigel DR, Steins M, Ready NE, et al. Nivolumab versus docetaxel in advanced nonsquamous non-small-cell lung cancer. N Engl J Med 2015;373:1627–39.
9. Brahmer J, Reckamp KL, Baas P, Crino L, Eberhardt WE, Poddubskaya E, et al. Nivolumab versus docetaxel in advanced squamous-cell non-small-cell lung cancer. N Engl J Med 2015;373:123–35.
10. Lievense LA, Sterman DH, Cornelissen R, Aerts JG. Checkpoint blockade in lung cancer and mesothelioma. Am J Respir Crit Care Med 2017;196:274–82.
11. Biton J, Ouakrim H, Dechartres A, Alifano M, Mansuet-Lupo A, Si H, et al. Impaired tumor-infiltrating T cells in patients with chronic obstructive pulmonary disease impact lung cancer response to PD-1 blockade. Am J Respir Crit Care Med 2018;198:928–40.
12. Mark NM, Kargl J, Busch SE, Yang GHY, Metz HE, Zhang H, et al. Chronic obstructive pulmonary disease alters immune cell composition and immune checkpoint inhibitor efficacy in non-small cell lung cancer. Am J Respir Crit Care Med 2018;197:325–36.
13. Nirmal AJ, Regan T, Shih BB, Hume DA, Sims AH, Freeman TC. Immune cell gene signatures for profiling the microenvironment of solid tumors. Cancer Immunol Res 2018;6:1388–400.
14. Chen PL, Roh W, Reuben A, Cooper ZA, Spencer CN, Prieto PA, et al. Analysis of immune signatures in longitudinal tumor samples yields insight into biomarkers of response and mechanisms of resistance to immune checkpoint blockade. Cancer Discov 2016;6:827–37.
15. Prat A, Navarro A, Pare L, Reguart N, Galvan P, Pascual T, et al. Immune-related gene expression profiling after PD-1 blockade in non-small cell lung carcinoma, head and neck squamous cell carcinoma, and melanoma. Cancer Res 2017;77:3540–50.
16. Ayers M, Lunceford J, Nebozhyn M, Murphy E, Loboda A, Kaufman DR, et al. IFN-gamma-related mRNA profile predicts clinical response to PD-1 blockade. J Clin Invest 2017;127:2930–40.
17. Keohavong P, Kahkonen B, Kinchington E, Yin J, Jin J, Liu X, et al. K-ras mutations in lung tumors from NNK-treated mice with lipopolysaccharide-elicited lung inflammation. Anticancer Res 2011;31:2877–82.
18. Eisenhauer EA, Therasse P, Bogaerts J, Schwartz LH, Sargent D, Ford R, et al. New response evaluation criteria in solid tumours: revised RECIST guideline (version 1.1). Eur J Cancer 2009;45:228–47.
19. Newman AM, Liu CL, Green MR, Gentles AJ, Feng W, Xu Y, et al. Robust enumeration of cell subsets from tissue expression profiles. Nat Methods 2015;12:453–7.
20. Becht E, Giraldo NA, Lacroix L, Buttard B, Elarouci N, Petitprez F, et al. Estimating the population abundance of tissue-infiltrating immune and stromal cell populations using gene expression. Genome Biol 2016;17:218.
21. Abbas AR, Baldwin D, Ma Y, Ouyang W, Gurney A, Martin F, et al. Immune response in silico (IRIS): immune-specific genes identified from a compendium of microarray expression data. Genes Immun 2005;6:319–31.
22. Angelova M, Charoentong P, Hackl H, Fischer ML, Snajder R, Krogsdam AM, et al. Characterization of the immunophenotypes and antigenomes of colorectal cancers reveals distinct tumor escape mechanisms and novel targets for immunotherapy. Genome Biol 2015;16:64.
23. Watkins NA, Gusnanto A, de Bono B, De S, Miranda-Saavedra D, Hardie DL, et al. A HaemAtlas: characterizing gene expression in differentiated human blood cells. Blood 2009;113:e1–9.
24. Bindea G, Mlecnik B, Tosolini M, Kirilovsky A, Waldner M, Obenauf AC, et al. Spatiotemporal dynamics of intratumoral immune cells reveal the immune landscape in human cancer. Immunity 2013;39:782–95.
25. Rutz S, Noubade R, Eidenschenk C, Ota N, Zeng W, Zheng Y, et al. Transcription factor c-Maf mediates the TGF-beta-dependent suppression of IL-22 production in T(H)17 cells. Nat Immunol 2011;12:1238–45.
26. Aken BL, Achuthan P, Akanni W, Amode MR, Bernsdorff F, Bhai J, et al. Ensembl 2017. Nucleic Acids Res 2017;45:D635–D42.
27. Fridlender ZG, Sun J, Mishalian I, Singhal S, Cheng G, Kapoor V, et al. Transcriptomic analysis comparing tumor-associated neutrophils with granulocytic myeloid-derived suppressor cells and normal neutrophils. PLoS One 2012;7:e31524.
28. Bronte V, Brandau S, Chen SH, Colombo MP, Frey AB, Greten TF, et al. Recommendations for myeloid-derived suppressor cell nomenclature and characterization standards. Nat Commun 2016;7:12150.
29. Loukinova E, Dong G, Enamorado-Ayalya I, Thomas GR, Chen Z, Schreiber H, et al. Growth regulated oncogene-alpha expression by murine squamous cell carcinoma promotes tumor growth, metastasis, leukocyte infiltration and angiogenesis by a host CXC receptor-2 dependent mechanism. Oncogene 2000;19:3477–86.
30. Melkamu T, Qian X, Upadhyaya P, O'Sullivan MG, Kassie F. Lipopolysaccharide enhances mouse lung tumorigenesis: a model for inflammation-driven lung cancer. Vet Pathol 2013;50:895–902.
31. Qian X, Khammanivong A, Song JM, Teferi F, Upadhyaya P, Dickerson E, et al. RNA-sequencing studies identify genes differentially regulated during inflammation-driven lung tumorigenesis and targeted by chemopreventive agents. Inflamm Res 2015;64:343–61.
32. Durham AL, Adcock IM. The relationship between COPD and lung cancer. Lung Cancer 2015;90:121–7.
33. Barnes PJ. Inflammatory mechanisms in patients with chronic obstructive pulmonary disease. J Allergy Clin Immunol 2016;138:16–27.
34. Young RP, Hopkins RJ, Christmas T, Black PN, Metcalf P, Gamble GD. COPD prevalence is increased in lung cancer, independent of age, sex and smoking history. Eur Respir J 2009;34:380–6.
35. Venaille T, Snella MC, Holt PG, Rylander R. Cell recruitment into lung wall and airways of conventional and pathogen-free guinea pigs after inhalation of endotoxin. Am Rev Respir Dis 1989;139:1356–60.
36. Kips JC, Tavernier J, Pauwels RA. Tumor necrosis factor causes bronchial hyperresponsiveness in rats. Am Rev Respir Dis 1992;145:332–6.
37. Michel O, Ginanni R, Le Bon B, Content J, Duchateau J, Sergysels R. Inflammatory response to acute inhalation of endotoxin in asthmatic patients. Am Rev Respir Dis 1992;146:352–7.
38. Rylander R, Bake B, Fischer JJ, Helander IM. Pulmonary function and symptoms after inhalation of endotoxin. Am Rev Respir Dis 1989;140:981–6.
39. Moghaddam SJ, Li H, Cho SN, Dishop MK, Wistuba II, Ji L, et al. Promotion of lung carcinogenesis by chronic obstructive pulmonary disease-like airway

inflammation in a K-ras-induced mouse model. Am J Respir Cell Mol Biol 2009; 40:443–53.
40. Takahashi H, Ogata H, Nishigaki R, Broide DH, Karin M. Tobacco smoke promotes lung tumorigenesis by triggering IKKbeta- and JNK1-dependent inflammation. Cancer Cell 2010;17:89–97.
41. Chang SH, Mirabolfathinejad SG, Katta H, Cumpian AM, Gong L, Caetano MS, et al. T helper 17 cells play a critical pathogenic role in lung cancer. Proc Natl Acad Sci U S A 2014;111:5664–9.
42. Ronai ZA, Gradia S, Peterson LA, Hecht SS. G to A transitions and G to T transversions in codon 12 of the Ki-ras oncogene isolated from mouse lung tumors induced by 4-(methylnitrosamino)-1-(3-pyridyl)-1-butanone (NNK) and related DNA methylating and pyridyloxobutylating agents. Carcinogenesis 1993;14:2419–22.
43. Matzinger SA, Crist KA, Stoner GD, Anderson MW, Pereira MA, Steele VE, et al. K-ras mutations in lung tumors from A/J and A/J x TSG-p53 F1 mice treated with 4-(methylnitrosamino)-1-(3-pyridyl)-1-butanone and phenethyl isothiocyanate. Carcinogenesis 1995;16:2487–92.
44. Cancer Genome Atlas Research N. Comprehensive molecular profiling of lung adenocarcinoma. Nature 2014;511:543–50.
45. Herbst RS, Morgensztern D, Boshoff C. The biology and management of non-small cell lung cancer. Nature 2018;553:446–54.
46. Galon J, Bruni D. Approaches to treat immune hot, altered and cold tumours with combination immunotherapies. Nat Rev Drug Discov 2019;18:197–218.
47. Narayanapillai SC, Han YH, Song JM, Kebede ME, Upadhyaya P, Kassie F. Modulation of the PD-1/PD-L1 immune checkpoint axis during inflammation-associated lung tumorigenesis. Carcinogenesis 2020;41:1518–28.
48. Wherry EJ, Kurachi M. Molecular and cellular insights into T cell exhaustion. Nat Rev Immunol 2015;15:486–99.
49. Liu J, Hamrouni A, Wolowiec D, Coiteux V, Kuliczkowski K, Hetuin D, et al. Plasma cells from multiple myeloma patients express B7-H1 (PD-L1) and increase expression after stimulation with IFN-{gamma} and TLR ligands via a MyD88-, TRAF6-, and MEK-dependent pathway. Blood 2007;110:296–304.
50. Trujillo JA, Sweis RF, Bao R, Luke JJ. T cell-inflamed versus non-T cell-inflamed tumors: a conceptual framework for cancer immunotherapy drug development and combination therapy selection. Cancer Immunol Res 2018;6:990–1000.
51. Gabrilovich DI, Ostrand-Rosenberg S, Bronte V. Coordinated regulation of myeloid cells by tumours. Nat Rev Immunol 2012;12:253–68.
52. Highfill SL, Cui Y, Giles AJ, Smith JP, Zhang H, Morse E, et al. Disruption of CXCR2-mediated MDSC tumor trafficking enhances anti-PD1 efficacy. Sci Transl Med 2014;6:237ra67.
53. Clavijo PE, Moore EC, Chen J, Davis RJ, Friedman J, Kim Y, et al. Resistance to CTLA-4 checkpoint inhibition reversed through selective elimination of granulocytic myeloid cells. Oncotarget 2017;8:55804–20.
54. Sun L, Clavijo PE, Robbins Y, Patel P, Friedman J, Greene S, et al. Inhibiting myeloid-derived suppressor cell trafficking enhances T cell immunotherapy. JCI Insight 2019;4:e126853.

Cancer Research
The Journal of Cancer Research (1916–1930) | The American Journal of Cancer (1931–1940)

AACR American Association for Cancer Research

Lipopolysaccharide-Mediated Chronic Inflammation Promotes Tobacco Carcinogen–Induced Lung Cancer and Determines the Efficacy of Immunotherapy

Chia-Hsin Liu, Zhong Chen, Kong Chen, et al.

Cancer Res 2021;81:144-157. Published OnlineFirst October 29, 2020.